Chinese Chemical Letters 33 (2022) 2121–2124

Contents lists available at ScienceDirect

Chinese Chemical Letters

journal homepage: www.elsevier.com/locate/cclet

Ag-single atoms modified $S_{1.66}$-$N_{1.91}$/TiO_{2-x} for photocatalytic activation of peroxymonosulfate for bisphenol A degradation

Tian Wang[a], Jianjun Zhou[a], Wenjuan Wang[a], Yunqing Zhu[a,*], Junfeng Niu[a,b]

[a] School of Environmental Science and Engineering, Shaanxi University of Science and Technology, Xi'an 710021, China
[b] School of Environment and Civil Engineering, Dongguan University of Technology, Dongguan 523808, China

ARTICLE INFO

Article history:
Received 30 May 2021
Revised 2 July 2021
Accepted 18 August 2021
Available online 22 August 2021

Keywords:
Photo-Fenton
Single-atomic photocatalyst
Sulfate radical
Bisphenol A
PMS

ABSTRACT

In this study, $Ag_{0.23}$/($S_{1.66}$-$N_{1.91}$/TiO_{2-x}) single-atom photocatalyst was synthesized by *in-situ* photo-reducing of silver on S,N-TiO_{2-x} nanocomposite and used to degrade bisphenol A (BPA) through heterogeneous activation of potassium peroxymonosulfate (PMS) under visible-light illumination. The structure, physicochemical property, morphology, and electronic property were evalutated by X-ray diffraction (XRD), Raman spectrum, X-ray photoelectron spectra (XPS), high-resolution transmission electron microscopy (HR-TEM), UV–vis diffuse reflectance spectra (UV-vis DRS), electron paramagnetic resonance (EPR) spectrum. $Ag_{0.23}$/($S_{1.66}$-$N_{1.91}$/TiO_{2-x}) single-atom photocatalyst exhibited 2.4 times higher activity for the synergetic degradation of BPA than that of its counterpart, and 48.73% mineralization rate of BPA also achieved. It was ascribed to the uniformly-dispersed metallic Ag atoms as the active site for accelerating the migration rate of photo-generated carrier for generation of high reactive radicals. The EPR experiments indicated that $SO_4^{\bullet-}$ and $^{\bullet}OH$ was jointly involved in BPA degradation.

Bisphenol A (BPA) is well-known as an endocrine-disrupting chemical (EDC) that can mimic estrogen and interact with its receptors. It has great potential to cause hazardous health and ecologic effects even at doses lower than the safety level (50 mg kg^{-1} day^{-1} by FDA [1-3]. In the past two decades, BPA has been widely used in manufacturing plastics, paper, medical equipment, electronics, and clothes, and every year more than 6.0×10^9 pounds of BPA are produced [4,5]. Therefore, it is necessary to find an efficient and environmentally friendly treatment method to eliminate BPA.

Fenton-like process is promised as an efficient technology for treatment of refractory organic pollutants because of its strong oxidation capability and environmental benignness [6,7]. Different from the traditional $^{\bullet}OH$ based Fenton technology, sulfate radicals ($SO_4^{\bullet-}$) for its high redox potential (E^0 = 2.5-3.1 eV) and selectively oxidation capability, has attracted plenty of attention in recent years [8,9]. In addition, for sulfate radical based Fenton-like technology, the 2-9 pH adoptive range and 30-40 μs half-life also made it more efficient in environmental remediation [10]. Furthermore, to increase its catalytic efficiency, several methods, like UV irradiation, transition metal ions (like Co^{2+}, Cu^{2+}, or Fe^{2+}) and metal oxides, have been proposed as approaches for accelerating the reaction of $SO_4^{\bullet-}$ generation [11-13].

Recently, photocatalytic Fenton process by coupling of potassium peroxymonosulfate (PMS) with photocatalysts for enhancing the $SO_4^{\bullet-}$ radicals generation has been studied as a new and efficient approach. TiO_2, Co_3O_4, $BiVO_4$, C_3N_4, and manganese oxide molecular sieve were all investigated as photo-Fenton catalysts for contaminants degradation under visible light irradiation [14-16]. However, the development of efficient and stable photocatalysts for the generation of $SO_4^{\bullet-}$ is still highly desired. Single-atom catalysts (SACs) by engineering the nanoparticle size to extremely small as single atom to achieve a maximum amount of unsaturated coordinated atoms have been widely studied in recent years [17,18]. The isolated atoms in SACs are unsaturatedly coordinated and exhibited unique physicochemical properties [19,20]. In the photocatalytic reaction, the atomically dispersed atoms are exposed in the reaction situation and participated in the reaction as high reactive sites [21]. So the atomic efficiency would be 100%, a maximum value in theory.

Herein, defective S, N-TiO_{2-x} with a large number of uniformly distributed surface oxygen vacancies was adopted as substrate for preparation of single-atom Ag photocatalysts. As shown in Fig. 1a, the $S_{1.66}$-$N_{1.91}$/TiO_{2-x} exhibits a lattice spacing of 0.37 nm corresponding to (101) facet of TiO_2 [22]. Compared with TiO_{2-x}, the lattice spacing is slightly increased (Fig. S1 in Supporting in-

* Corresponding author.
E-mail address: zhuyunqing@sust.edu.cn (Y. Zhu).

https://doi.org/10.1016/j.cclet.2021.08.085
1001-8417/

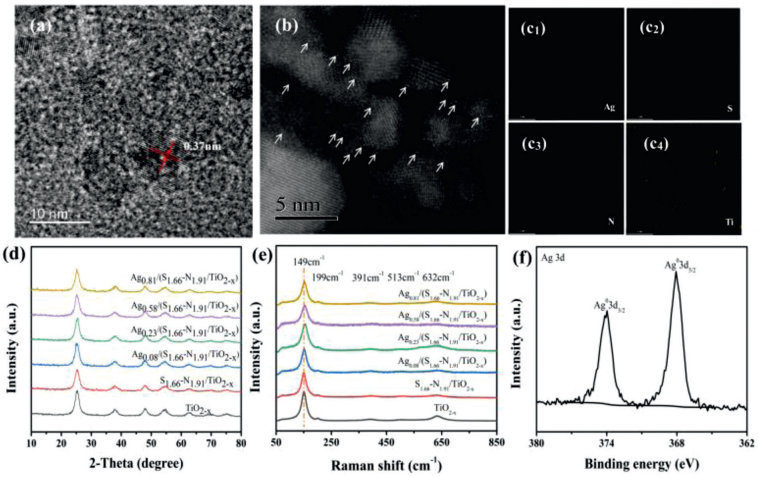

Fig. 1. (a) HRTEM diagram of $S_{1.66}$-$N_{1.91}$/TiO_{2-x}. (b) HAADF-STEM diagram of $Ag_{0.23}$/($S_{1.66}$-$N_{1.91}$/TiO_{2-x}). (c) Corresponding EDS mapping of Ag, S, N, Ti elements, respectively of $Ag_{0.23}$/($S_{1.66}$-$N_{1.91}$/TiO_{2-x}). (d) XRD pattern of Ag_z/($S_{1.66}$-$N_{1.91}$/TiO_{2-x}). (e) Raman spectra of Ag_z/($S_{1.66}$-$N_{1.91}$/TiO_{2-x}). (f) XPS spectra of $Ag_{0.23}$/($S_{1.66}$-$N_{1.91}$/TiO_{2-x}): Ag 3d.

formation) [23], which may be ascribed to the doping of sulfur and nitrogen. Fig. 1b is the HAADF-STEM diagram of $Ag_{0.23}$/($S_{1.66}$-$N_{1.91}$/TiO_{2-x}). It can be seen that Ag atoms exist as single atoms on the surface of the $S_{1.66}$-$N_{1.91}$/TiO_{2-x}, and the dispersion is uniform. From the EDS mapping images of $Ag_{0.23}$/($S_{1.66}$-$N_{1.91}$/TiO_{2-x}) (Fig. 1c), it can be seen that the four elements are uniformly distributed in the material. The Ag element was isolatedly dispersed on the surface, which further proves that the silver atoms are loaded successfully and are evenly distributed as silver atoms on $S_{1.66}$-$N_{1.91}$/TiO_{2-x} surface. The elements that S and N, Ag can be clearly observed in the EDS diagram of $Ag_{0.23}$/($S_{1.66}$-$N_{1.91}$/TiO_{2-x}), which proves the successful preparation of this material (Fig. S2 in Supporting information). As shown in Fig. 1d, the characteristic diffraction peaks of the prepared material Ag_z/($S_{1.66}$-$N_{1.91}$/TiO_{2-x}) are located at 25.3°, 37.8°, 48.1°, 53.9°, 55.1°, 62.7° and 75.0° respectively, corresponding to the (101), (004), (200), (105), (211), (204) and (215) crystal planes of the anatase phase TiO_{2-x} proved that the anatase phase photocatalytic material was successfully prepared [24,25]. Fig. 1e shows the Raman spectra of TiO_{2-x} and $S_{1.66}$-$N_{1.91}$/TiO_{2-x} with different Ag loadings. The characteristic Raman signal peak position of TiO_{2-x} was marked in Fig. S3 (Supporting information). It can be seen from the figure that the characteristic Raman signals are located at 149 cm^{-1}, 196 cm^{-1}, 391cm^{-1}, 513 cm^{-1}, 632 cm^{-1} [26]. There is the strongest Raman signal at 149 cm^{-1}, indicating that the prepared material exhibits the Raman characteristic band of anatase phase TiO_{2-x}. This result is consistent with X-ray diffraction (XRD) analysis. The Raman vibration mode of anatase TiO_{2-x} is 3Eg + 2B1g + A1g, and the oscillation peaks at 149 cm^{-1}, 196 cm^{-1} and 632 cm^{-1} correspond to the E_g vibration mode, the oscillation peak at 391 cm^{-1} and 513 cm^{-1} corresponds to the $B1_g$ oscillation mode [27]. Compared with the $S_{1.66}$-$N_{1.91}$/TiO_{2-x} Raman signal, the Raman band of Ag_z/($S_{1.66}$-$N_{1.91}$/TiO_{2-x}) shows no red shift or blue shift with the increase of Ag loading suggesting that the loading of Ag did not change the structure of $S_{1.66}$-$N_{1.91}$/TiO_{2-x}. Fig. 1f shows the high-resolution XPS peaks of Ag in Ag_z/($S_{1.66}$-$N_{1.91}$/TiO_{2-x}), as shown in this figure, the binding energies of Ag $3d_{5/2}$ and Ag $3d_{3/2}$ orbitals are 368.1 eV and 374.1 eV respectively [28]. The difference in binding energy between the two orbitals is 6 eV, indicating that Ag exists as zero valence state.

The g factor of the electron paramagnetic resonance (EPR) signal for all the samples (Fig. 2) is 2.003, which is classified into EPR signal of oxygen vacancies [29]. The $S_{1.66}$-$N_{1.91}$/TiO_{2-x} has the highest intensity of EPR signal, which indicated that the concentration of oxygen vacancies is highest in all the samples. After loading Ag

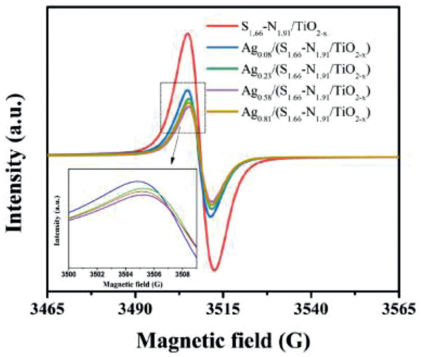

Fig. 2. EPR spectra of Ag_z/($S_{1.66}$-$N_{1.91}$/TiO_{2-x}).

species, the EPR signal intensity of oxygen vacancies gradually decreased with the increase of the loading amount of Ag. But when the loading amount of Ag is higher than 0.81%, it no longer follows the above-mentioned rules. This is due to the formation of Ag nanoclusters or nanoparticles on the surface of $S_{1.66}$-$N_{1.91}$/TiO_{2-x}, only a small amount of Ag occupies oxygen vacancies.

The transient photocurrent (15 μA/cm^2) of $S_{1.66}$-$N_{1.91}$/TiO_{2-x} is greater than that of pure TiO_{2-x} (12 μA/cm^2), this is due to the fact that S^{6+} can be reduced to more stable S^{4+} [30]. Doped S^{6+} can increase the separation rate of photo-generated electrons and holes. N replaces O^{2-} by bonding or enters into the crystal lattice to cause distortion of the TiO_{2-x} lattice. When S and N co-doping interaction in the TiO_{2-x} band gap, a new energy level is formed, which improves the separation efficiency of the catalyst for photo-generated carriers [31]. After Ag loading, $Ag_{0.08}$/($S_{1.66}$-$N_{1.91}$/TiO_{2-x}), $Ag_{0.23}$/($S_{1.66}$-$N_{1.91}$/TiO_{2-x}), $Ag_{0.58}$/($S_{1.66}$-$N_{1.91}$/TiO_{2-x}) and $Ag_{0.81}$/($S_{1.66}$-$N_{1.91}$/TiO_{2-x}) show the transient photocurrents of 28, 42, 23, 14 μA/cm^2, respectively (Fig. 3a). It was found that the transient photocurrent of $Ag_{0.23}$/($S_{1.66}$-$N_{1.91}$/TiO_{2-x}) was the largest, which was about 3.5 times that of TiO_{2-x} and 3 times that of $S_{1.66}$-$N_{1.91}$/TiO_{2-x}, indicating that single atom Ag can improve the separation rate of photo-generated electrons and holes [32], and in the photo-Fenton process, it can also increase the transport and capture photo-generated electrons. The DRS spectrum can further prove that the material $Ag_{0.23}$/($S_{1.66}$-$N_{1.91}$/TiO_{2-x}) has the highest light absorption (Fig. S4 in Supporting information). However, the increasing of Ag loading amount resulted a decreasing of transient photocurrent, which is due to the excessive Ag prior to form Ag particles with lower dispersity and low-density

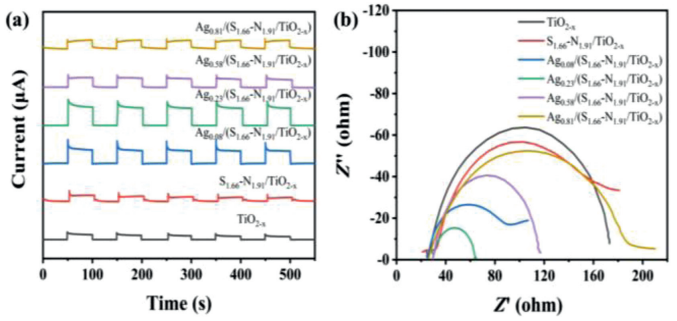

Fig. 3. (a) Transient photocurrent response. (b) EIS Nyquist plots of $Ag_z/(S_{1.66}\text{-}N_{1.91}/TiO_{2\text{-}x})$.

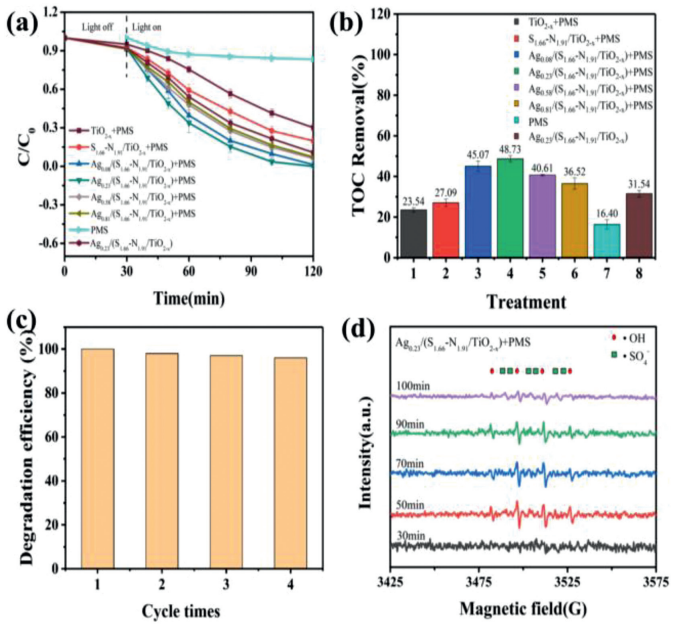

Fig. 4. Photo-Fenton degradation of BPA by $Ag_z/(S_{1.66}\text{-}N_{1.91}/TiO_{2\text{-}x})$ activated persulfate. (a) Typical time course of BPA concentration. (b) Histogram of TOC removal. (c) Catalyst recycling for the photodegradation of BPA. (d) EPR spectra of free radical.

of carrier separation centers. It can be seen from Fig. 3b that the radius of the electrochemical impedance spectroscopy curve of the $S_{1.66}\text{-}N_{1.91}/TiO_{2\text{-}x}$ modified by co-doping of $TiO_{2\text{-}x}$ with S and N is small, indicating that the electrochemical impedance is small and the interface charge transfer is faster, and the separation effect of photo-generated electrons and holes is better [33]. Compared with pure $S_{1.66}\text{-}N_{1.91}/TiO_{2\text{-}x}$ electrochemical impedance, the Ag-loaded $S_{1.66}\text{-}N_{1.91}/TiO_{2\text{-}x}$ ($Ag_z/(S_{1.66}\text{-}N_{1.91}/TiO_{2\text{-}x})$) light Fenton catalytic materials have low electrochemical impedance, relatively fast interface charge transfer, and long carrier lifetime [34]. The electrochemical impedance of the single-atom catalytic material $Ag_{0.23}/(S_{1.66}\text{-}N_{1.91}/TiO_{2\text{-}x})$ is the smallest, which is nearly 1/4 of the electrochemical impedance of $S_{1.66}\text{-}N_{1.91}/TiO_{2\text{-}x}$, is maximized the atomic utilization rate, it can make the separation effect of photo-generated electrons and holes best, which is conducive to the improvement of catalytic activity.

The photo-Fenton degradation of BPA at initial concentration of 15 mg/L with molar ratios of Oxone to BPA at 2.2 is shown in Fig. 4a. In case of PMS under visible light irradiation, no obvious degradation of BPA was observed. By activation of PMS in dark with $Ag_{0.23}/(S_{1.66}\text{-}N_{1.91}/TiO_{2\text{-}x})$, 53.88% of BPA and 19.73% of total organic carbon (TOC) were removed after 120 minutes of contact time (Fig. 4b). Once visible light irradiation was applied, 100% of BPA and 48.73% of TOC were removed at the end of treatment. Based on the data, the degradation of BPA was fitted with the pseudo-first order kinetic model (Fig. S5 in Supporting information), and the kinetic constant was 0.032 min^{-1} which is two to three times higher than its counterpart. While comparing the catalysts with different Ag loading amount, $Ag_{0.23}/(S_{1.66}\text{-}N_{1.91}/TiO_{2\text{-}x})$ displayed the highest catalytic efficiency of BPA and TOC removal in the 120 min reaction. Tables S1 and S2 (Supporting information) listed the BPA and TOC removal of all samples in the photo-Fenton-like process. It suggested that the high catalytic efficiency was ascribed to the isolated silver atoms in the single atom catalysts. The cycling test (Fig. 4c) implied that $Ag_{0.23}/(S_{1.66}\text{-}N_{1.91}/\ TiO_{2\text{-}x})$ SAC shown high stability in the photo-Fenton degradation of BPA, and after four times cycling experiments, the catalytic efficiency only shown slightly decrease.

The EPR spectrum was used to detect the active radicals during the photo-Fenton degradation of BPA with $Ag_{0.23}/(S_{1.66}\text{-}N_{1.91}/TiO_{2\text{-}x})$ using DMPO as spin trapping agent. As shown in Fig. 4d, the signals of DMPO-OH and DMPO-SO_4 adducts were both observed in the reaction. It means that $^{\bullet}OH$ and $SO_4^{\bullet-}$ co-participate in the degradation process of BPA [35,36]. With the time increasing, the signal intensity was firstly enhanced and then reduced. It agreed with the reaction trend that during the initial stage of the reaction, the generated active radicals were fast reacted with BPA molecule resulting in a high reaction rate, and EPR spectum showed no singal. After 30 min, the reaction rate decreased and the DMPO trapped radicals were increased. The $SO_4^{\bullet-}$ reacted with H_2O to form plenty of $^{\bullet}OH$. So the signal intensity was enhanced correspondingly. Then at the end of reaction, PMS was used up. The signal of the radicals were both reduced, which further confirmed that the $^{\bullet}OH$ was generated from $SO_4^{\bullet-}$ [37].

In this work, the single atomic photocatalysts were successfully prepared and tested in the photo-Fenton-like system for BPA degradation under visible-light irradiation. In this system, the SACs labeled as $Ag_{0.23}/(S_{1.66}\text{-}N_{1.91}/TiO_{2\text{-}x})$ possessed high-efficiency for photo-generated carrier separation and transportation, which resulted in a high yield of $SO_4^{\bullet-}$ radicals and also the conversion to $^{\bullet}OH$ for effective mineralization of BPA. Meanwhile, photocatalytic process promoted the reduction of the isolated Ag atoms from Ag^+ to Ag^0 to ensure the efficient activation of PMS.

Declaration of competing interest

The authors have no conflicts of interest to declare.

Acknowledgments

Thia work is financial supported by the National Nature Science Foundation of China (No. 21876105), Key Research & Development Program Projects of Shaanxi Province (No. 2019SF-252), the Startup Foundation for Advanced Talents of Shaanxi University of Science and Technology.

Supplementary materials

Supplementary material associated with this article can be found, in the online version, at doi:10.1016/j.cclet.2021.08.085.

References

[1] H. Wang, L.P. Liu, J.Y. Wang, et al., Sci. Total Environ. 601 (2017) 1733–1742.
[2] Y. Shang, X. Xu, B.Y. Gao, S.B. Wang, X.G. Duan, Chem. Soc. Rev. 50 (2021) 5281–5322.
[3] P.P. Qiu, T. Zhao, X.H. Zhu, et al., Chin. Chem. Lett. 32 (2021) 1456–1461.
[4] K.A. Thayer, D.R. Doerge, D. Hunt, et al., Environ. Int. 83 (2015) 107–115.
[5] P. Ye, D.M. Wu, M.Y. Wang, et al., Appl. Surf. Sci. 428 (2018) 131–139.
[6] D. Meral, Ultrason. Sonochem. 40 (2018) 110–116.
[7] J.L. Wang, S.Z. Wang, Chem. Eng. J. 334 (2018) 1502–1517.

[8] Y. Soltanabadi, M. Jourshabani, Z. Shariatinia, Sep. Purif. Technol. 202 (2018) 227–241.
[9] Y. Shang, X. Xu, Q.Y. Yue, B.Y. Gao, Y.W. Li, Environ. Sci. 7 (2020) 1444–1453.
[10] X.M. Lei, M.H. You, F. Pan, et al., Chin. Chem. Lett. 30 (2019) 2216–2220.
[11] F. Chen, X. Jiang, L. Zhang, R. Lang, B. Qiao, Chin. J. Catal. 39 (2018) 893–898.
[12] H. Zhang, G. Liu, L. Shi, J. Ye, Adv. Energy Mater. 8 (2018) 1701343.
[13] T. Wang, Y.Q. Zhu, Z.Y. Luo, Y.X. Li, C.Y. Wang, Environ. Chem. Lett. 19 (2021) 1815–1821.
[14] Y.Q. Zhu, T. Wang, T. Xu, Y.X. Li, C.Y. Wang, Appl. Surf. Sci. 464 (2019) 36–42.
[15] F. Chen, X.L. Wu, L. Yang, et al., Chem. Eng. J. 394 (2020) 124904.
[16] A. Abdelhaleem, W. Chu, Chem. Eng. J. 338 (2018) 411–421.
[17] Y.Q. Zhu, W.J. Wang, et al., Environ. Chem. Lett. 17 (2018) 481–486.
[18] M. Taherinia, M. Nasiri, E. Abedini, H.R. Pouretedal, J. Iran. Chem. Soc. 15 (2018) 1301–1310.
[19] A. Kadam, T. Salunkhe, H. Kim, S.W. Lee, Appl. Surf. Sci. 518 (2020) 169–4332.
[20] A. Brindha, T. Sivakumar, J. Photochem. Photobiol. A 340 (2017) 146–156.
[21] Y.H. Tian, Y.Z. Wu, Q.Y. Yi, et al., Chem. Eng. J. 128644 (2021) 1385–8947.
[22] P.O. Diez, S. Giannakis, J. Rodríguez-Chueca, et al., Water Res. 186 (2020) 116387.
[23] L. Devi, M. Srinivas, M.L. ArunaKumari, J. Water Process Eng. 13 (2016) 117–126.
[24] T. Soltani, A. Tayyebi, B. Lee, Appl. Surf. Sci. 441 (2018) 853–861.
[25] B.F. Zhang, M.T. Zhang, L. Zhang, et al., J. Colloid Interface Sci. 594 (2021) 635–649.
[26] H.B. Qiu, P.C. Guo, L. Yuan, G.P. Sheng, Chin. Chem. Lett. 31 (2020) 2614–2618.
[27] J.J. Qi, J.Z. Liu, F.B. Sun, et al., Chin. Chem. Lett. 32 (2021) 1814–1818.
[28] H. Yu, L. Ye, T. Zhang, H. Zhou, T. Zhao, RSC Adv. 7 (2017) 15265–15271.
[29] X. Kong, Z. Peng, R. Jiang, et al., ACS Appl. Nano Mater. 3 (2020) 1373–1381.
[30] G.H. Li, Y.Y. Sun, Q.M. Zhang, et al., Chem. Eng. J. 410 (2021) 128397.
[31] T. Li, A. Abdelhaleem, W. Chu, et al., Chem. Eng. J. 411 (2021) 128450.
[32] T. Suwannaruang, P. Kidkhunthod, N. Chanlek, S. Soontaranon, K. Wantala, Appl. Surf. Sci. 478 (2019) 1–14.
[33] J. Wang, G.H. Wang, B. Cheng, J.G. Yu, J.J. Fan, Chin. J. Catal. 42 (2021) 56–68.
[34] R.T. Bento, O.V. Correa, M.F. Pillis, Mater. Chem. Phys. 261 (2021) 124231.
[35] Y.K. Park, B.J. Kim, S.M. Jeong, et al., Environ. Res. 188 (2020) 109630.
[36] N. Kovalevskiy, D. Selishchev, D. Svintsitskiy, et al., Catal. Commun. 134 (2020) 105841.
[37] X.Q. An, Q.W. Tang, H.C. Lan, H.J. Liu, J.H. Qu, Appl. Catal. B 244 (2019) 407–413.